Enhancement of mechanical properties of heat-resistant martensitic steel processed by equal channel angular pressing

G. Yang [a,*], C.X. Huang [b,*], C. Wang [a], L.Y. Zhang [a], C. Hu [a], Z.F. Zhang [b], S.D. Wu [b]

[a] Central Iron and Steel Research Institute, Beijing 100081, China
[b] Shenyang National Laboratory for Materials Science, Institute of Metal Research, Chinese Academy of Sciences, Shenyang 110016, China

ARTICLE INFO

ABSTRACT

The microstructures and tensile properties of a commercial heat-resistant martensitic steel processed by equal channel angular pressing (ECAP) for one pass and subsequent ageing treatment were investigated. Both optical and TEM examinations showed that many martensite laths had been broken into dislocation cells and subgrains after ECAP deformation. At the same time, the fragmentation of rod-shaped precipitates was also observed and the distribution of precipitation was more uniform than that in the as-received sample. After ageing in the temperature range of 640–720 °C for 2 h, dislocation recovery took place resulting in the decrease of dislocation density and formation of many ultrafine grains with sizes of several hundred of nanometers, and spherical particles that were uniformly dispersed in the matrix of fine subgrains/grains. By ECAP deformation and subsequent ageing treatment, a simultaneous increase in both strength and toughness was achieved, compared with those of as-received state. The enhancement of tensile properties was attributed to microstructural refinement and uniform distribution of precipitates.

© 2009 Elsevier B.V. All rights reserved.

1. Introduction

Severe plastic deformation (SPD), which can impose large accumulative plastic strain (>1), is currently attractive method to produce ultrafine grained (UFG) metallic materials [1,2]. Typical SPD techniques include equal channel angular pressing (ECAP) [1–3], accumulative roll bonding [4], high pressure torsion [2,5], and surface mechanical attrition treatment [6]. Due to its unique capacity for producing bulk samples with sizes of centimetres, ECAP has received much attention during the past two decades [1–3,7,8]. A prominent profit of microstructural refinement induced by SPD is of great enhancement of strength. The yield strengths of UFG Cu, Fe and low carbon steels are several times higher than those of their coarse-grained counterparts [1,2,7–11]. However, as well known, the ductility, particularly uniform elongation of the as-deformed materials processed by ECAP even for one pass, is undesirably low at room temperature, which severely inhibits their applications in industry [2,7–11]. Therefore, the as-deformed materials were usually submitted to subsequent thermal–mechanical treatments in order to improve their ductility. Annealing is a traditional and very important thermal treatment, which can lead to dislocation recovery and recrystallization. For example, UFG-Cu was annealed at

about 200 °C for 3 min and obtained a bi-model grain structure [12]. As a result, its uniform elongation was substantially improved, whereas its strength was sacrificed little [12]. Another important thermal–mechanical treatment developed in recent years is the composite deformations, i.e. two kinds of severe plastic deformation sometimes together with annealing are applied to the same material. The typical composite deformations are ECAP plus severe cold rolling. Wang et al. [13] and Stolyarov et al. [14] have used this method to deform Cu, Fe and Ti, and finally obtained excellent mechanical properties, such as high strength combined with high ductility and high impact toughness at very low temperature.

For some precipitation-hardened alloys, the effect of ECAP deformation on precipitation and their mechanical properties is significant. The fragmentation of precipitates was observed in some Al alloys, such as θ'-precipitants in an Al–Cu alloy [15] and β'-precipitants in an Al–Mg–Si alloy [16]. Recently, several investigations have shown that the treatment of ECAP deformation plus subsequent low-temperature ageing was very effective in enhancing room temperature tensile properties of some precipitation-hardened al alloys [17–20]. For instance, the yield strength of 2024 Al alloy treated by ECAP deformation and subsequent ageing at low temperature was higher by a factor of about 1.3 than that of the T351 treated 2024 Al alloy, whereas the ductility was comparable [21].

In addition to SPD methods, several advanced thermal–mechanical processes were also developed in recently years in order to obtain UFG microstructures in steels. Song et al. have

* Corresponding authors. Tel.: +86 10 6218 2760; fax: +86 10 6218 2795.
E-mail addresses: yanggang@nercast.com (G. Yang), chxhuang@imr.ac.cn (C.X. Huang).

Table 1
Chemical composition of the heat-resistant martensitic steel in this investigation.

Elements	C	Cr	Ni	Co	W	Mo	V	Nb	N	Fe
Concentration (wt.%)	0.15	15.71	2.1	4.85	0.84	1.32	0.24	0.30	0.048	Balance

given an overview of processing, microstructure and mechanical properties of UFG steels produced by means of SPD methods and advanced thermal–mechanical processes [22]. Different from SPD methods, advanced thermal–mechanical processes pursue alternative strategies to produce UFG microstructures. These strategies include dynamic recrystallization of ferrite during warm deformation [23], pronounced recovery of ferrite during warm deformation and annealing [24,25], and strain-induced phase transformation by cold rolling and subsequent annealing [26], etc.

In this work, a commercial heat-resistant martensitic steel was selected, as it is representative for martensitic lamellar structure and precipitation-hardened material. It should also be noted that heat-resistant martensitic steel is a kind of difficult-work steels and its processing through ECAP is technically challenging.

2. Experimental procedure

A hot-rolled heat-resistant matensitic steel was used in this investigation. The chemical composition of the material is given in Table 1. The hot-rolled rods were firstly treated at 1100 °C for 1 h and quenched in oil to obtain martensitic lamellar structure. Then, the rods were divided into three groups (A, B and C) and submitted to ageing at 640, 680 and 720 °C for 2 h, respectively, and the samples were denoted as A_0, B_0 and C_0. For ECAP processing, the samples were cut from the as-received rods with dimensions of Ø 8 mm × 45 mm and denoted as A_E, B_E and C_E. Table 2 gives the processing conditions of tested samples in the present work.

The ECAP procedure was carried out using a split die with two channels intersecting at inner angle of 90° and outer angle of 30°, which yields an effective strain of ∼1 by a single pass. The samples lubricated with MoS_2 were pressed for only one pass at room temperature. Repetitive pressing of the same sample was attempted by using route Bc [27]. However, it was failed due to severe cracking by shear mode during the second pressing. After the first pressing, the samples were artificially aged at 640, 680 and 720 °C for 2 h, and the samples denoted as A_{E+aged}, B_{E+aged} and C_{E+aged}, respectively.

Samples for optical microscope and transmission electron microscope (TEM, JEM-2000FX II) examinations were cut from the transverse cross-sections of the as-pressed rods. Thin foils for TEM were firstly mechanically ground to about 50 μm thick and then thinned by a twin-jet polishing facility using a solution of 5% perchloric acid and 95% ethanol at −20 °C.

Tensile specimens with a dog-bone shape were cut from the as-pressed rods with the tensile axes oriented parallel to the extru-sion direction. The gauge dimension of tensile specimen was Ø 3 mm × 15 mm. Tensile experiments were performed on an Instron 8871 testing machine at a constant crosshead speed of 1 mm/min at room temperature.

3. Results and discussion

3.1. Microstructures

3.1.1. Optical microstructures

Fig. 1(a) shows the initial optical microstructures of as-received sample B_0. The microstructures are characterized by equiaxed grains with an average grain size of 30 μm. Within grains, martensite laths are arrayed regularly and the lath boundaries (LBs) are very sharp. The initial optical microstructures and grain sizes of samples A_0 and C_0 are as similar as those of sample B_0.

Fig. 1(b) is the optical microstructures of sample B_E processed by ECAP for one pass. It can be seen that both grain boundaries (GBs) and martensite LBs blur out. Obviously, plastic deformation has been imposed upon martensite laths. Compared with the optical microstructures of sample B_E, there are no apparent differences of the microstructures of samples A_E and C_E, which were also deformed by ECAP for one pass. The as-pressed samples were then submitted to ageing treatments at 640, 680 and 720 °C for 2 h, and the corresponding optical microstructures are presented in Fig. 1(c)–(e), respectively. It can be observed that both GBs and martensite LBs become clearer than that observed in the as-deformed samples, suggesting the occurrence of microstructure recovery.

3.1.2. TEM microstructures

Fig. 2(a) is the typical bright-field TEM micrograph of as-received sample B_0, showing the initial microstructures of GB and martensite lath. It is clear that most laths are straight and LBs are sharp. For the as-received condition of samples A_0, B_0 and C_0, measurements showed that the largest martensite laths could be ∼3 μm in width, but the very thin laths was only ∼50 nm in width. Close inspection shows that a lot of precipitates gather at GBs and LBs, as shown in Fig. 2(b). They are identified as $M_{23}C_6$ particles, as confirmed by the corresponding selected-area diffraction pattern with [−1 1 2] zone axis in Fig. 2(c). Measurements showed that the largest rod-shaped $M_{23}C_6$ precipitates had lengths and widths of ∼570 and ∼60 nm, respectively, whereas the very fine particles had dimensions of the order of ∼10 nm. In addition to the main precipitate $M_{23}C_6$, there were also other kinds of precipitants, such as MC. However, they were too small (<10 nm) to be observed in the complex microstructures of the present steel.

After ECA pressing for one pass at room temperature, most matensite laths were severely deformed and broken into subgrains or dislocation cells. Fig. 3(a) and (b) shows the typical microstructures of deformed matensite laths and subgrains/dislocation cells in low magnification, respectively, observed in sample B_E. High dislocation density was produced within subgrains and dislocation cells, as seen in Fig. 3(c) enlarged from the white frame in Fig. 3(b). Examinations show that most subgrains and dislocation cells have dimensions of 200–600 nm. The precipitates were again indentified after ECAP deformation and the TEM micrograph is shown in Fig. 3(d), in which the precipitates are indicated by arrows. It can be seen that the rod-shaped precipitates have become fragmented by the high pressure during ECAP, regardless of large and
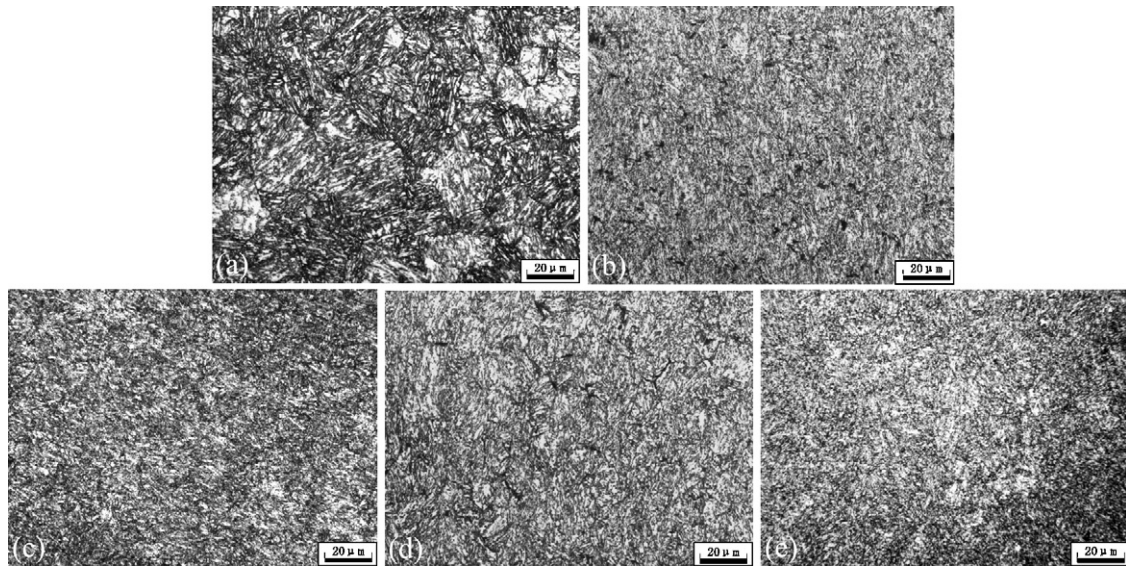
Table 2
Processing conditions of tested samples in the present work.

Samples	Heat treatment
Group A	
A_0	1100 °C × 1 h oil cooling; +640 °C × 2 h, air cooling
A_E	Deformed by ECAP for one pass
A_{E+aged}	Deformed by ECAP for one pass + aged at 640 °C for 2 h, air cooling
Group B	
B_0	1100 °C × 1 h oil cooling; +680 °C × 2 h air cooling
B_E	Deformed by ECAP for one pass
B_{E+aged}	Deformed by ECAP for one pass + aged at 680 °C for 2 h, air cooling
Group C	
C_0	1100 °C × 1 h oil cooling; +720 °C × 2 h air cooling
C_E	Deformed by ECAP for one pass
C_{E+aged}	Deformed by ECAP for one pass + aged at 720 °C for 2 h, air cooling

Fig. 1. Optical microstructures of samples treated by different conditions: (a) as-received sample B_0; (b) sample B_E, ECAP-deformed; (c) sample A_{E+aged}, ECAP-deformed + 640 °C × 2 h; (d) sample B_{E+aged}, ECAP-deformed + 680 °C × 2 h; (e) sample C_{E+aged}, ECAP-deformed + 720 °C × 2 h.

small ones. Furthermore, accompanied with the deformation of matensite laths, the particles are more randomly distributed, but not narrowed only at GBs and LBs.

Fig. 4(a)–(g) presents the typical TEM microstructures of samples A_{E+aged}, B_{E+aged} and C_{E+aged}, which were aged at 640, 680 and 720 °C for 2 h, respectively, after ECAP deformation. For sample A_{E+aged}, the microstructures keep the deformation microstructures but with lower dislocation density, and some matensite laths can also be detected, as shown in Fig. 4(a). However, more close examination shows that many ultrafine grains/subgrains appear even within martensite laths, as shown in Fig. 4(b) enlarged from the white frame in Fig. 4(a). It is found that these ultrafine grains/subgrains are in elongated shape with mean length and width of ∼500 and ∼200 nm, respectively. The formation of ultrafine grains/subgrains should be attributed to dislocation recovery that results in the transformation from subgrains/dislocation cells to ultrafine grains/subgrains [28–30]. Fig. 4(c) shows the microstructures of sample B_{E+aged}. It is found that more ultrafine grains are produced, while matensite laths are hardly observed. Different from the ultrafine grains observed in sample A_{E+aged}, the grains in sample B_{E+aged} are a little bigger and more equiaxed, as seen in Fig. 4(d) enlarged from the white frame in Fig. 4(c). The mean size is about 300 nm. When aged at 720 °C, the deformation microstructures are completely replaced by fine equiaxed subgrains/grains, as shown in Fig. 4(e) and (f). It is seen that many grains are almost dislocation free. The mean size of these fine subgrains/grains is about 800 nm. Besides, recrystallization grains with size of several micrometers are also observed somewhere in sample C_{E+aged}, as shown in Fig. 4(g). From the above observations, the microstructures of the samples processed by ECAP exhibit several important characteristics during ageing treatment. One is the formation of many ultrafine grains, which should be due to dis-
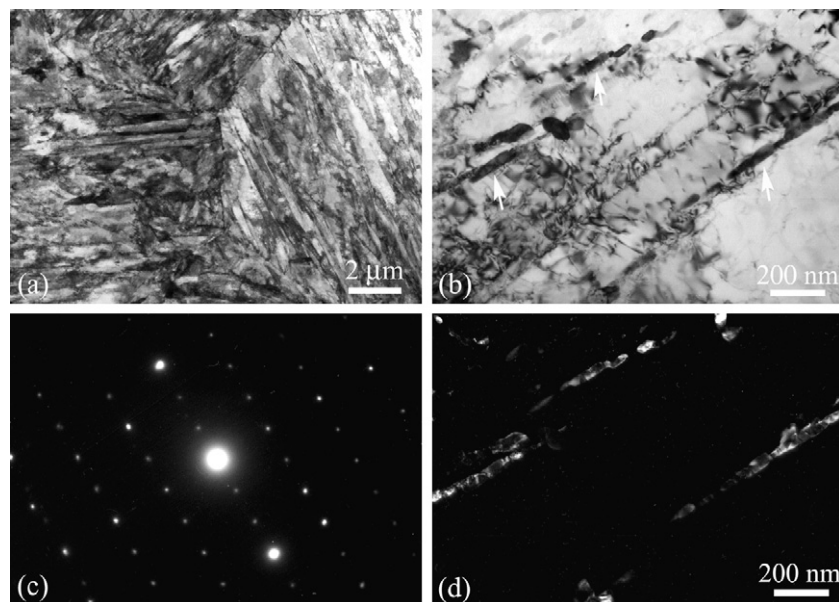

Fig. 2. TEM microstructures of as-received sample B_0: (a) bright-field image with low magnification; (b) bright-field image with high magnification, the arrows indicate precipitants along the boundaries of martensite lathes; (c) selected-area diffraction pattern of precipitants ($M_{23}C_6$) with zone axis [−1 1 2]; (d) dark-field image of precipitants.
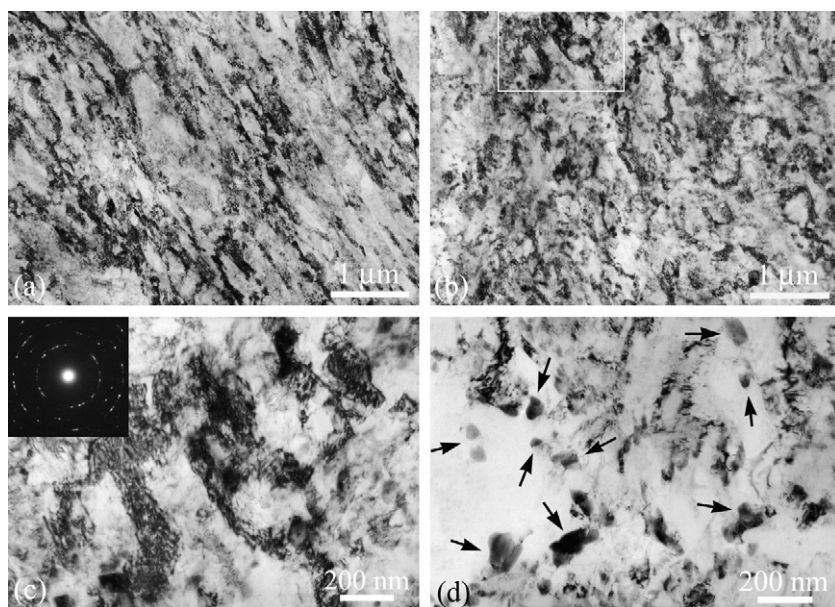
Fig. 3. TEM micrographs of sample B_E processed by ECAP for one pass: (a) martensitic laths; (b) dislocation cells and subgrains; (c) an enlarged image from the white frame in (b); and (d) $M_{23}C_6$ precipitants indicated by black arrows.

location recovery leading to the transformation from dislocation cells/subgrains to ultrafine grains. Another characteristic is that with increasing the ageing temperature, the grains became bigger and the dislocation density is lower.

In addition to the formation of ultrafine grains and the decrease of dislocation density, the third important observation is the very fine spherical particles, which are randomly distributed in the matrix of fine subgrains/grains. After ageing treatment, the sharp edges and corners of particles produced by the fragmentation of rod-shaped precipitates (seeing Fig. 3(d)) have been removed, resulting in spherical particles as shown in Fig. 5(a)–(c). Furthermore, the particles show more smooth contours in the sample aged at high temperature than that in the sample aged at low temperature. It is reasonable to believe that partial dissolution of these precipitates has taken place during ageing. The influence of ECAP deformation on the dissolution of precipitants has been investigated in some Al alloys and low-carbon steels previously [29,31–33]. For Al alloys, it was found that dissolution was more favored and could occur at a lower temperature after many passes of ECAP deformation, because the precipitates had been fully fragmented so that they dissolved more readily [32]. In low-carbon steels pressed by ECAP, pearlite particles could be completely decomposed to form fine, uniformly distributed cementie precipitants by static annealing [33].

3.2. Tensile properties

The typical tensile engineering stress–strain curves of tested samples are shown in Fig. 6(a)–(c) and their corresponding mechanical properties are presented in the form of histogram in Fig. 7(a)–(c). Table 3 further gives the values of ultimate tensile strength (σ_{UTS}), yield strength ($\sigma_{0.2}$, 0.2% proof stress), elongation-to-fracture (δ), cross-sectional area reduction (A) and static toughness (U) of all tested samples. For as-received samples (curves A_0, B_0 and C_0), their tensile properties are very similar. The yield strength is 920–940 MPa and the elongation to fracture is ∼15.5%. After ECAP processing for one pass, the yield strength can be increased to 1400 MPa, but also sacrificed the entire uniform plastic deformation, as shown by the curves A_E, B_E and C_E in Fig. 6(a)–(c). By means of ageing treatment, the samples obtain the

ability of uniform plastic deformation again and therefore their ductilities are increased, though their strengths decrease a little. The A_{E+aged} sample has very high yield strength (1345 MPa) together with good ductility. With increasing the ageing temperature, the strength decreases further but the ductility increases. For sample C_{E+aged}, both strength and elongation to fracture are a little higher than those of as-received sample C_0. The most optimization of tensile properties is of sample B_{E+aged}, which exhibits the same elongation to fracture as that of the as-received sample B_0 but much higher strength.

In order to value the tensile properties of the present material comprehensively, the parameter of static toughness is used. In general, static toughness indicates a combination of strength and ductility and it can be calculated by

$$U = \int_0^{\varepsilon_f} \sigma \cdot d\varepsilon,$$

where σ is the flow stress and ε_f is the total strain at fracture. Fig. 7 and Table 3 show the variation of static toughness of heat-resistant martensitc steel in different states. It can be seen that the static toughness of as-received samples is ∼160 mJ/m². After ECAP

Table 3
Ultimate tensile strength (σ_{UTS}), yield strength ($\sigma_{0.2}$, 0.2% proof stress), elongation-to-fracture (δ), cross-sectional area reduction (A) and static toughness (U) of heat-resistant martensitc steel in different processing conditions. Each value was averaged from the data of two tested samples.

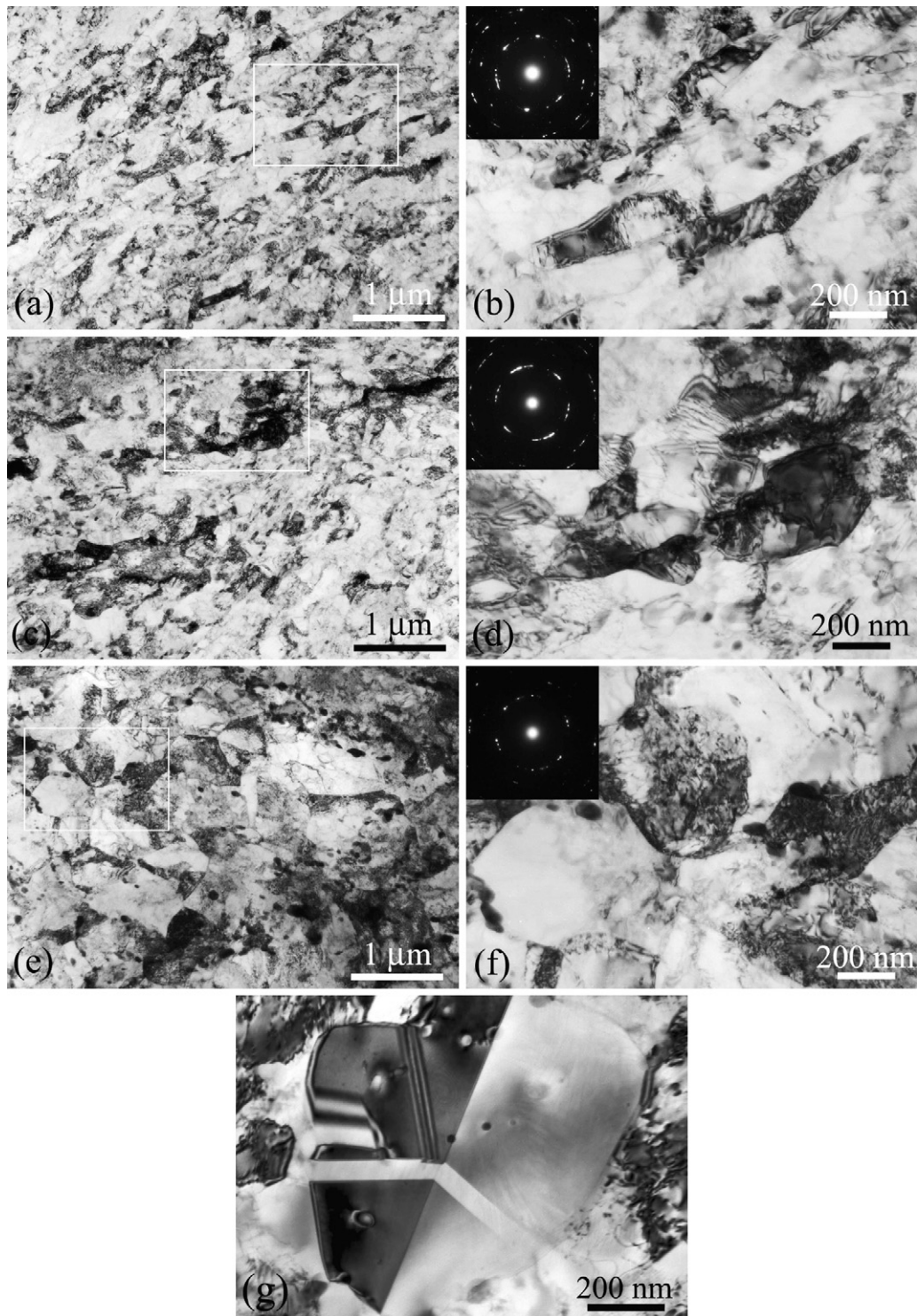| Samples	σ_{UTS} (MPa)	$\sigma_{0.2}$ (MPa)	δ (%)	A (%)	U (mJ/m²)
Group A					
A_0	1197	942	15.5	57.8	164
A_E	1482	1434	8.5	42.8	112
A_{E+aged}	1413	1345	13.1	46.3	173
Group B					
B_0	1157	922	15.7	60.3	160
B_E	1454	1400	8.6	42.2	109
B_{E+aged}	1337	1037	15.2	57.9	182
Group C					
C_0	1171	928	15.7	58.2	163
C_E	1461	1421	8.0	39.4	108
C_{E+aged}	1227	962	16.9	56.1	184

Fig. 4. TEM micrographs of different samples: (a) and (b) A_{E+aged}, ECAP-deformed + 640 °C × 2 h; (c) and (d) B_{E+aged}, ECAP-deformed + 680 °C × 2 h; (e)–(g) C_{E+aged}, ECAP-deformed + 720 °C × 2 h. Images (b), (d) and (f) are enlarged from the white frames in (a), (c) and (e), respectively.

deformation for one pass, its value decreases significantly down to ∼110 mJ/m^2. Obviously, it is due to the loss of uniform plastic deformation, though the strength is improved. The static toughness can be recovered by ageing treatment. Moreover, it should be noted that the static toughness of all aged samples are higher than those of their as-received counterparts. For samples B_{E+aged} and C_{E+aged}, the values can reach 180 mJ/m^2, which is higher by a factor of about 1.13 than those of samples B_0 and C_0. It can be explained that the ductility, especially the uniform plastic defor-

mation, is recovered to the same level as that of the as-received state whereas the strength is still higher. Thus, it is suggested that it is feasible to adjust the mechanical properties of material by ECAP processing and subsequent ageing treatment.

The present tested steel is a kind of martensitic precipitation-hardened steel. The high strength, combined with good toughness, is achieved by martesitic lamellar structure and fine precipitants which are uniformly distributed in martensitic matrix. By means of single-pass ECAP processing and subsequent ageing treatment,
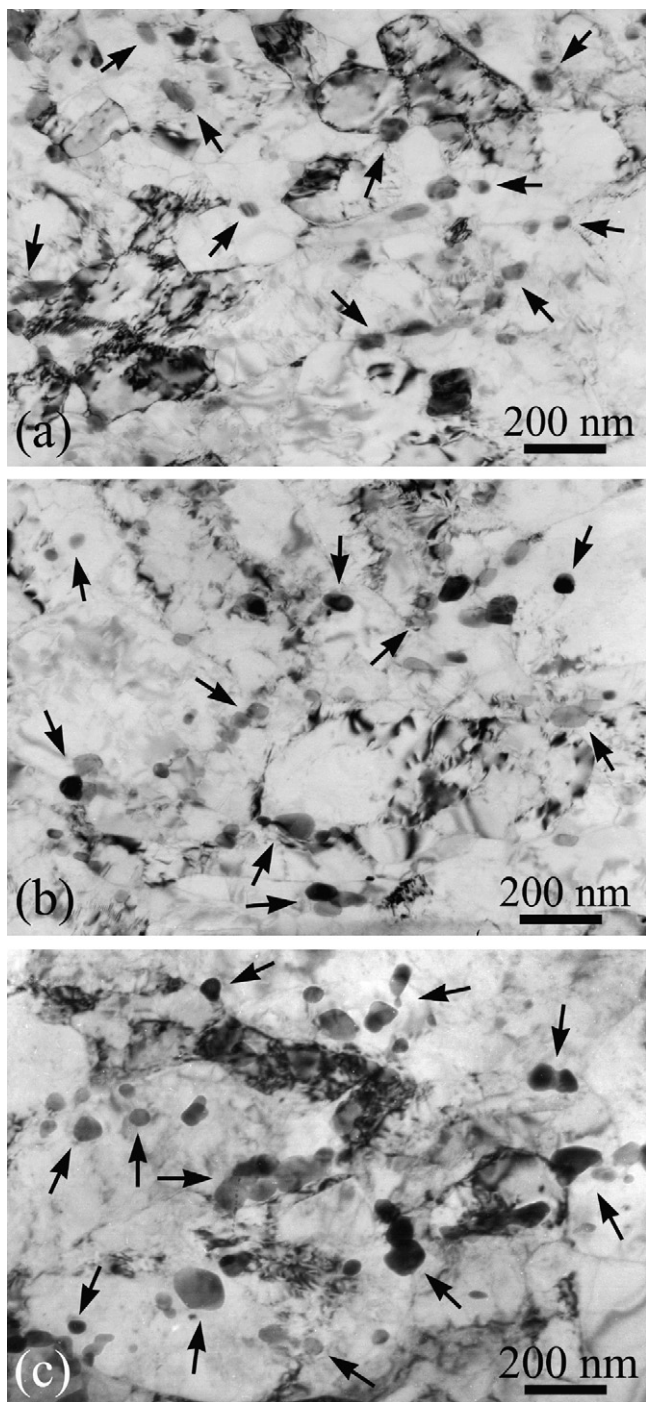
Fig. 5. TEM micrographs showing spherical precipitates in samples: (a) A_{E+aged}, ECAP-deformed + 640 °C × 2 h; (b) B_{E+aged}, ECAP-deformed + 680 °C × 2 h; (c) C_{E+aged}, ECAP-deformed + 720 °C × 2 h. The precipitates are indicated by arrows.

Fig. 6. Tensile engineering stress–strain curves of tested samples: (a) group A, treated at 640 °C; (b) group B, treated at 680 °C; (c) group C, treated at 720 °C.

a simultaneous enhancement of both strength and ductility was achieved in the present heat-resistant martensitic steel. Several factors should contribute to the improvement of tensile properties. One is the refined subgrain/grain structure. By ECAP deformation, high dislocation density was produced in martensite laths, resulting in the severe deformation of laths. Accordingly, the sample lost strain hardening ability, leading to early necking, which is very similar to most of the metals pressed by ECAP [1–3,7,8]. After subsequent ageing treatment, ultrafine subgrains/grains with low dislocation density formed. Though the strength decreased, the ductility was increased mainly because of the increase in uniform
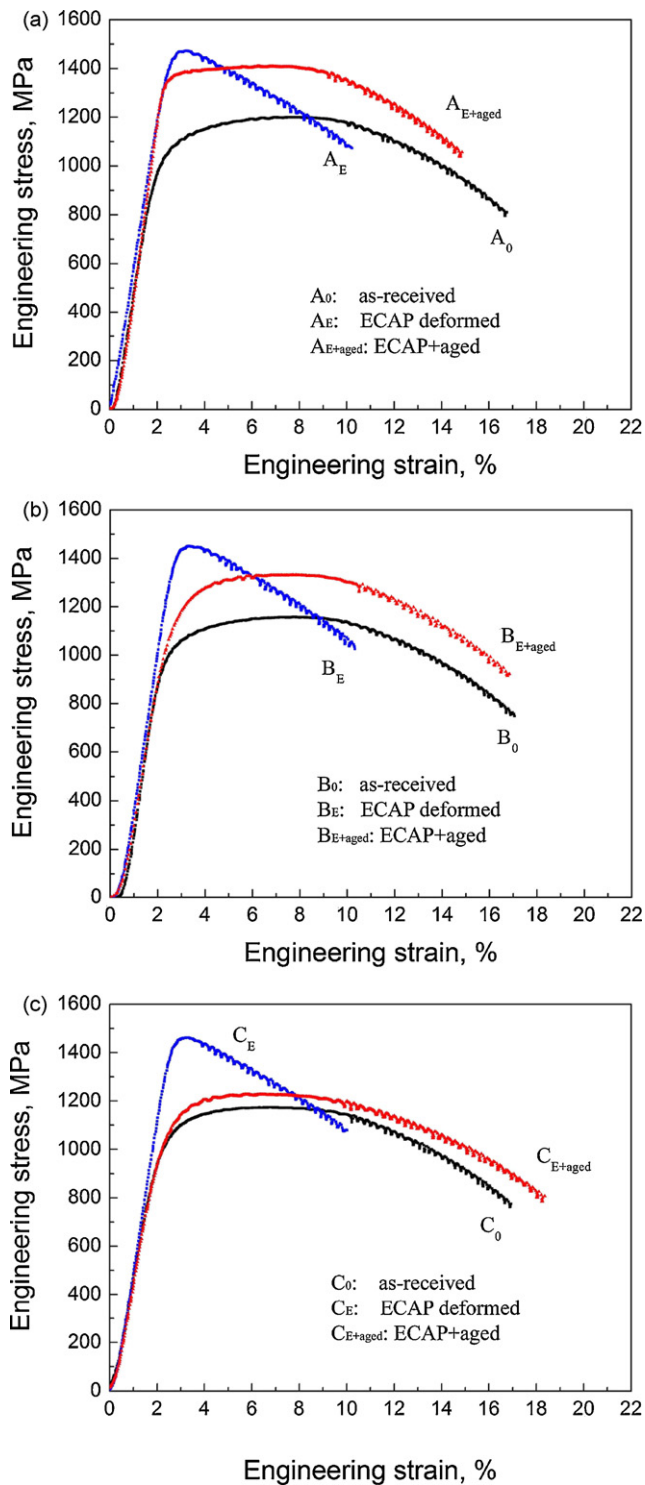
plastic deformation. It is suggested that the refined subgrain/grain structure in the present material can provide not only high strength but also high strain hardening ability. Fig. 8 shows the strain hardening exponents of the tested samples. It is found that the values of the samples processed by ECAP and subsequent ageing treatment can be comparable to that of the as-received state. The regained strain hardening ability can sustain large uniform plastic deformation. The second factor is the many fine spherical particles. After ECAP processing and subsequent ageing treatment, the rod-shaped pre-
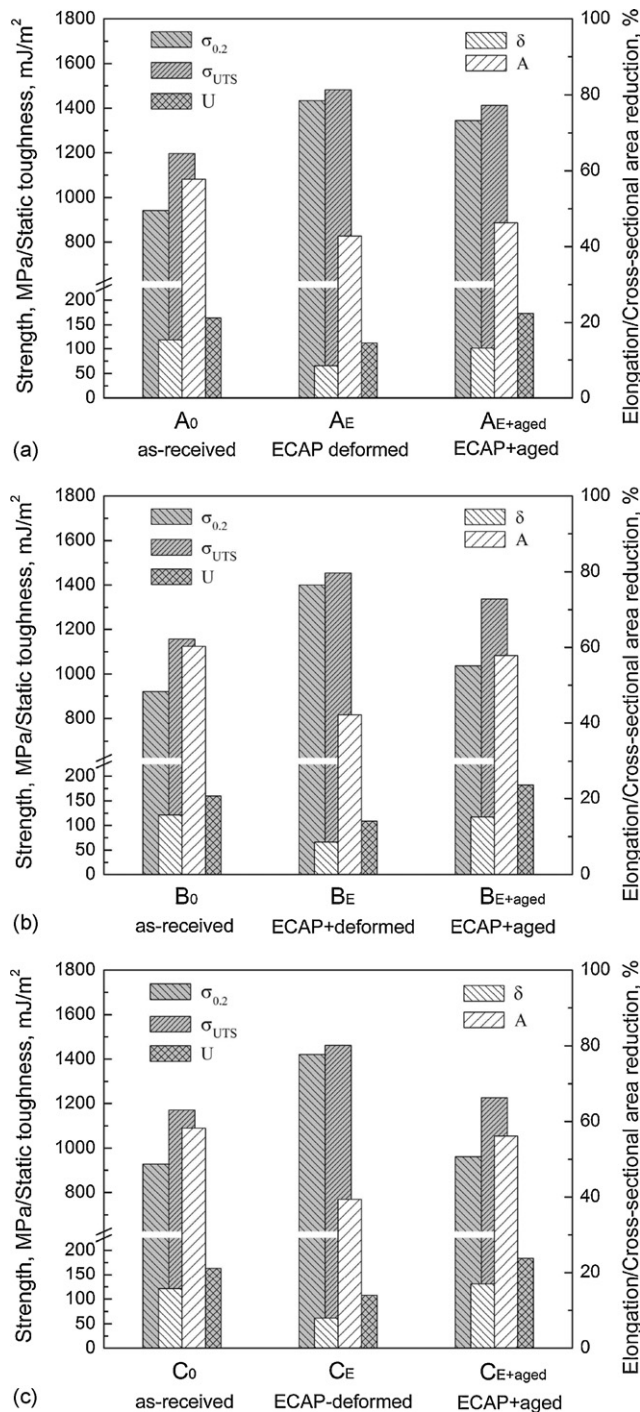
(a)

(b)

(c)

Fig. 7. Histograms of yield strength ($\sigma_{0.2}$), ultimate tensile strength (σ_{UTS}), static toughness (U), elongation-to-fracture (δ) and cross-sectional area reduction (A) for tested samples: (a) group A, treated at 640 °C; (b) group B, treated at 680 °C; (c) group C, treated at 720 °C.

Fig. 8. Strain hardening exponents of tested samples derived from $\ln\sigma - \ln\varepsilon$ plots. Samples: A_{E+aged}, ECAP-deformed + 640 °C × 2 h; B_{E+aged}, ECAP-deformed + 680 °C × 2 h; C_{E+aged}, ECAP-deformed + 720 °C × 2 h; B_0, as-received.

shown that the ultrafine and nanometer grain structures could offer a higher resistance to shear localization and shear fracture, and stabilize the hydrostatic triaxial stress state that promoted ductile fracture through microvoid nucleation and coalescence [14,34–37].

4. Conclusion

(1) A heat-resistant martensitic steel was successfully processed by ECAP for one pass at room temperature. By ECAP processing, martensite laths were severely deformed and broken into dislocation cells/subgrains, and the rod-shaped precipitants became fragmented too. After subsequent ageing treatment, ultrafine subgrains/grains in sizes of several hundred nanometers formed due to dislocation recovery. Partial dissolution of precipitates occurred during ageing, resulting in spherical particles which were more uniformly distributed in the matrix of fine subgrains/grains.

(2) A simultaneous improvement of both strength and ductility was achieved in heat-resistant martensitic steel processed by ECAP and subsequent ageing treatment. The refined subgrain/grain structures and more uniformly distributed fine precipitates can provide not only high strength but also strong strain hardening ability to sustain uniform plastic deformation.

Acknowledgements

References

[1] R.Z. Valiev, R.K. Islamgaliev, I.V. Alexandrov, Prog. Mater. Sci. 45 (2000) 103.
[2] R.Z. Valiev, T.G. Longdon, Prog. Mater. Sci. 51 (2006) 881.
[3] V.M. Segal, Mater. Sci. Eng. A281 (2002) 1.
[4] N. Tsuji, R. Ueji, Y. Minamino, Scripta Mater. 47 (2002) 69.
[5] Y. Ivanisenko, W. Lojkowski, R.Z. Valiev, H.J. Fecht, Acta Mater. 51 (2003) 5555.
[6] K. Lu, J. Lu, Mater. Sci. Eng. A375 (2004) 38.
[7] F.H. Dalla Torre, R. Lapovok, K.T. Remesh, P.F. Thomson, C.H.J. Davies, E.V. Pereloma, Acta Mater. 52 (2004) 481.
[8] C.X. Huang, G. Yang, B. Deng, S.D. Wu, S.X. Li, Z.F. Zhang, Philos. Mag. 87 (2007) 4949.
[9] C.X. Huang, S.D. Wu, S.X. Li, Z.F. Zhang, Adv. Eng. Mater. 10 (2008) 434.
[10] B.Q. Han, E.J. Lavernia, F.A. Mohamed, Metall. Mater. Trans. A34 (2003) 71.
[11] Y. Fukuda, K. Oh-ishi, Z. Horita, T.G. Langdon, Acta Mater. 50 (2002) 1359.

cipitants became fragmented into many finer spherical particles, i.e. increasing the precipitant density. Moreover, different from the distribution of precipitates only at GBs and LBs in the as-received state, these very fine particles were more uniformly distributed in the matrix of fine grains. The higher density and more uniformly distributed fine particles provided more obstructions to dislocation slip and thus increased the flow stress. Besides, together with the refined subgrain/grain structure, they might also reduce the size of nucleating flaws and increase the resistance to crack propagation, leading to a higher fracture stress. Many observations have
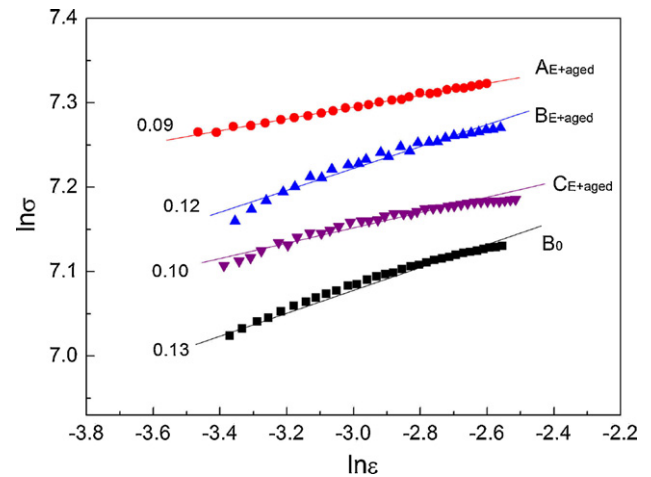
[12] Y.M. Wang, M.W. Chen, F.H. Zhou, E. Ma, Nature 419 (2002) 912.
[13] Y.M. Wang, E. Ma, R.Z. Valiev, Y.T. Zhu, Adv. Mater. 16 (2004) 328.
[14] V.V. Stolyarov, R.Z. Valiev, Y.T. Zhu, Appl. Phys. Lett. 88 (2006) 041905.
[15] M. Murayama, Z. Horita, K. Hono, Acta Mater. 49 (2001) 21.
[16] K. Oh-ishi, Y. Hashi, A. Sadakata, K. Kaneko, Z. Horita, T.G. Langdon, Mater. Sci. Forum 396–402 (2002) 333.
[17] J.K. Kim, H.G. Jeong, S.I. Hong, Y.S. Kim, W.J. Kim, Scripta Mater. 45 (2001) 901.
[18] Z. Horita, K. Oh-ishi, T. Fujita, K. Kaneko, T.G. Langdon, Adv. Mater. 17 (2005) 1599.
[19] Y.H. Zhao, X.Z. Liao, Y.T. Zhu, R.Z. Valiev, J. Mater. Res. 20 (2005) 288.
[20] S. Cheng, Y.H. Zhao, Y.T. Zhu, E. Ma, Acta Mater. 55 (2007) 5822.
[21] W.J. Kim, C.S. Chung, D.S. Ma, S.I. Hong, H.K. Kim, Scripta Mater. 49 (2003) 333.
[22] R. Song, D. Ponge, D. Raabe, J.G. Speer, D.K. Matlock, Mater. Sci. Eng. A441 (2006) 1.
[23] S.V.S. Murty, S. Torizuka, K. Nagai, T. Kitai, Y. Kogo, Scripta Mater. 53 (2005) 763.
[24] R. Song, D. Ponge, D. Raabe, Acta Mater. 53 (2005) 4881.
[25] B. Poorganji, G. Miyamoto, T. Maki, T. Furuhara, Scripta Mater. 59 (2008) 279.
[26] Y.Q. Ma, J.E. Jin, Y.K. Lee, Scripta Mater. 52 (2005) 1311.
[27] Y.T. Zhu, T.C. Lowe, Mater. Sci. Eng. A291 (2000) 46.
[28] D.H. Shin, B.C. Kim, K.-T. Park, W.Y. Choo, Acta Mater. 48 (2000) 3245.
[29] K.-T. Park, D.H. Shin, Mater. Sci. Eng. A 334 (2002) 79.
[30] D.G. Morris, M.A. Munoz-Morris, Acta Mater. 50 (2002) 4047.
[31] M.J. Strink, N. Gao, M. Furukawa, Z. Hortia, C. Xu, T.G. Langdon, Rev. Adv. Mater. Sci. 7 (2004) 1.
[32] N. Gao, M.J. Starink, M. Furukawa, Z. Horita, C. Xu, T.G. Langdon, Mater. Sci. Eng. A410–A411 (2005) 303.
[33] D.H. Shin, Y.S. Kim, E.J. Lavernia, Acta Mater. 49 (2001) 2387.
[34] Y.M. Wang, E. Ma, M.C. Chen, Appl. Phys. Lett. 80 (2002) 2395.
[35] A. Vinogradov, T. Ishida, K. Kitagawa, V.I. Kopylov, Acta Mater. 53 (2005) 2181.
[36] Y.G. Ko, D.H. Shin, K.T. Park, C.S. Lee, Scripta Mater. 54 (2006) 1785.
[37] D.R. Fang, Q.Q. Duan, N.Q. Zhao, J.J. Li, S.D. Wu, Z.F. Zhang, Mater. Sci. Eng. A459 (2005) 137.